



Study on adsorption properties and mechanism of thallium onto titanium iron magnetic adsorbent



Jiali Tang^a, Wanlin Wu^a, Ling Yu^b, Xiaoyun Fan^a, Guoqiang Liu^a, Yang Yu^{a,*}

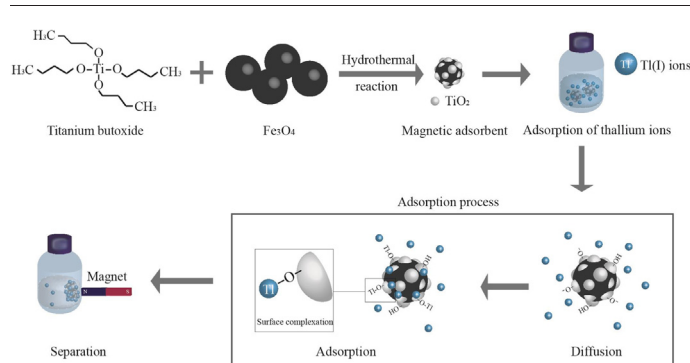
^a Guangdong key laboratory of Environmental Pollution and Health, School of Environment, Jinan University, Guangzhou 511443, China

^b Analysis and Test Center, Guangdong University of Technology, Guangzhou 511443, China

HIGHLIGHTS

- Particle size of magnetic adsorbent becomes smaller after hydrothermal reaction.
- q_{max} of Tl(I) is much higher than most of previously reported adsorbents.
- Over 83% of ultimate Tl(I) uptake can be achieved within the first 30 min.
- Competitive adsorption is mainly determined by ion electronegativity.
- Tl(I) ions are adsorbed on the adsorbent via the mechanism of surface complexation.

GRAPHICAL ABSTRACT



ARTICLE INFO

Article history:

Received 30 May 2019

Received in revised form 16 July 2019

Accepted 26 July 2019

Available online 27 July 2019

Editor: Xinbin Feng

Keywords:

Thallium

Adsorption

Magnetic adsorbent

Titanium

Hydrothermal synthesis

Mechanism

ABSTRACT

Thallium (Tl) contamination caused by the industrial wastewater leakage has become a serious environmental problem due to thallium's high toxicity. In this study, a novel titanium iron magnetic nano-sized adsorbent was synthesized and applied for the effective removal of thallium(I). The physicochemical properties of the adsorbent were investigated by a series of techniques such as scanning electron microscope (SEM), X-ray powder diffraction (XRD) and X-ray photoelectron spectroscopy (XPS). About 83% of equilibrium adsorption capacity could be accomplished within the initial 30 min. The adsorption of Tl(I) was found to be highly dependent on solution pH. The maximum adsorption capacity of Tl(I) was 111.3 mg/g at pH 7.0. The presence of such co-existing cations as Na^+ , Mg^{2+} , Ca^{2+} and Cu^{2+} could have a certain influence on the uptake of Tl(I). The adsorption mechanism was proposed as a surface complexation process of Tl(I) ions by binding to deprotonated sites of hydroxyl groups on the adsorbent surface. The prepared magnetic adsorbent would be suitable for effectively treating thallium-containing water due to its promising adsorption ability towards Tl(I) and ease in operation.

© 2019 Published by Elsevier B.V.

1. Introduction

Thallium (Tl) as a rare and highly toxic heavy metal element has been detected at the ng/L level in nature environment (Cheam et al., 1995; Lin and Nriagu, 1999). However, higher concentration of thallium in water can be caused by anthropogenic activities such as ore

* Corresponding author.

E-mail address: yuyang@jnu.edu.cn (Y. Yu).

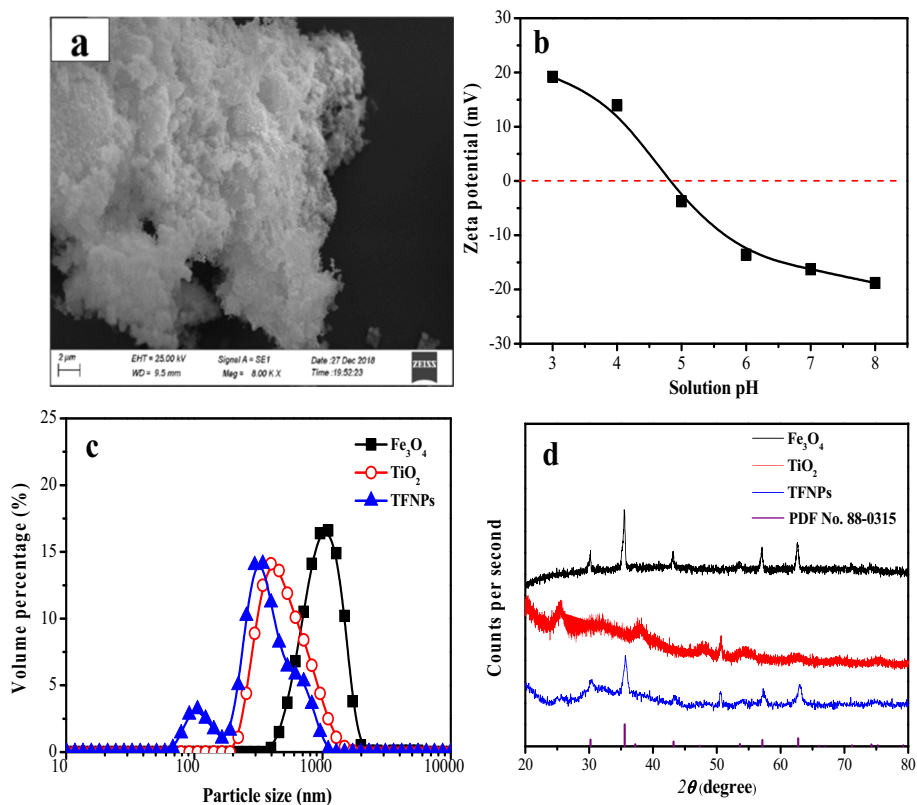


Fig. 1. SEM image (a) and zeta potential (b) of TFNPs; particle size distribution (c) and XRD patterns (d) of Fe₃O₄, TiO₂ and TFNPs.

processing, metal mining, smelting and coal combustion (Campanella et al., 2017; Peter and Viraraghavan, 2005; Williams-Beam and Twidwell, 2003). The maximum contaminant level (MCL) of thallium in drinking water was set as 2 μg/L by the US Environmental Protection Agency (USEPA) in 1992.

Thallium in water mainly exists in inorganic forms of thallium(I) and thallium(III). Though Tl(III) is more toxic than Tl(I), Tl(I) is more stable and soluble than Tl(III) (Mulkey and Oehme, 1993; Ralph and Twiss, 2002; Li et al., 2019). Therefore, the effective removal of Tl(I) from water has become a challenging issue. Compared to other technologies, adsorption is considered as the most promising method for the thallium removal because of its high efficiency, cost-effectiveness and ease in operation. Numerous adsorbents have been developed and utilized for the removal of thallium, including sawdust (Memon et al., 2008), activated carbon (Rivera-Utrilla et al., 2010), multi-walled carbon nanotubes (Pu et al., 2013), titanate nanotubes (Liu et al., 2014), nano-Al₂O₃ (Zhang et al., 2008) and titanium peroxide (Zhang et al., 2018). Among them, the highest removal of Tl(I) was reportedly achieved by titanate nanotubes (TNTs) at pH 5.0 through an ion-exchange process between Tl⁺ and Na⁺ or H⁺ in the inter layers of TNTs (Liu et al., 2014). At the neutral pH, titanium peroxide particles exhibited a Tl(I) adsorption capacity as high as 412 mg/g (Zhang et al., 2018). Difficulty in post-treatment is always the major disadvantage for above-mentioned adsorbents in practice applications. Energy-consuming centrifuge or filtration is required for separating those spent adsorbents after the treatment. In contrast, magnetic adsorbents can be simply separated from treated water under an external magnetic field in which the operation energy consumption can be greatly reduced. In order to improve the adsorption performance, other adsorptive materials with strong and special affinity towards target pollutants are generally incorporated into typical magnetic materials (e.g., Fe₃O₄ and Fe₂O₃) (Chandra et al., 2010; Ning et al., 2018; Zhang et al., 2010). Development and performance of magnetic adsorbents for other toxic substances such as arsenic (Tang et al.,

2013), cadmium (Feng et al., 2010) and mercury (Pan et al., 2012) have been extensively studied in the literature. Although some magnetic adsorbents were also reported for the removal of Tl(I) recently (Li et al., 2018a; Li et al., 2018b), more efforts are still urgently needed to be devoted to developing effective magnetic adsorbent with rapid adsorption rate and excellent adsorption capacity.

In this study, a new titanium iron nanoparticles (TFNPs) were synthesized by the hydrothermal method for thallium decontamination. The physicochemical properties of the adsorbent and adsorption mechanism were investigated by a variety of techniques including SEM, XRD and XPS. The adsorption kinetics, isotherm, influences of solution pH and co-existing cations and regeneration study were also examined.

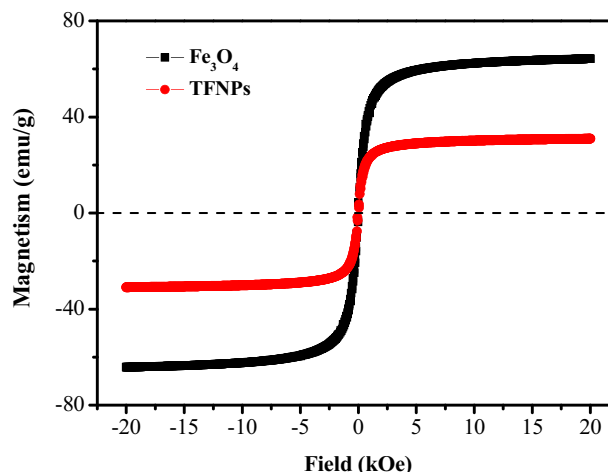


Fig. 2. Magnetism of Fe₃O₄ and TFNPs.

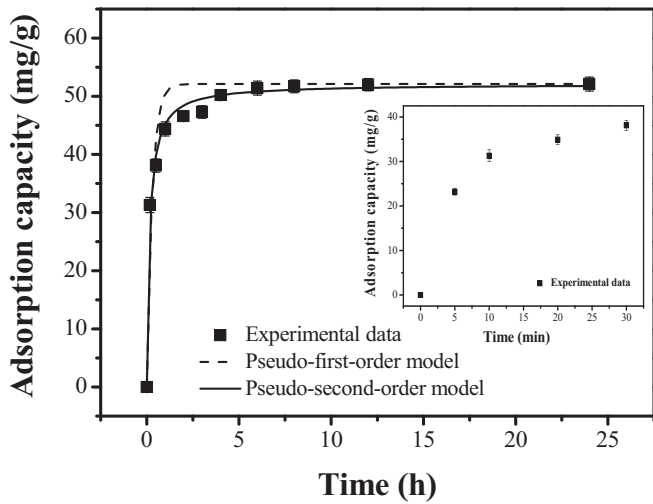


Fig. 3. Kinetics of Tl(I) adsorption on TFNPs at pH 7.0 (Insert graph: adsorption kinetics in 30 min). Experiment conditions: $[Tl(I)]_0 = 12.5 \text{ mg/L}$; adsorbent dosage = 0.1 g/L; $T = 25 \pm 1 \text{ }^\circ\text{C}$.

2. Materials and methods

2.1. Materials

The chemicals used in adsorbent preparation and adsorption studies including iron(III) nitrate nonahydrate ($\text{Fe}(\text{NO}_3)_3 \cdot 9\text{H}_2\text{O}$, >98.0%), iron (II) sulfate heptahydrate ($\text{FeSO}_4 \cdot 7\text{H}_2\text{O}$, >99.0%), titanium butoxide ($\text{C}_{16}\text{H}_{36}\text{O}_4\text{Ti}$, >99.0%), sodium hydroxide (NaOH , >98.0%), nitric acid (HNO_3 , 70%), thallium(I) nitrate (TiNO_3 , >99.9%), sodium chloride (NaCl , >99.5%), manganese chloride hexahydrate ($\text{MgCl}_2 \cdot 6\text{H}_2\text{O}$, >99.0%), calcium chloride dihydrate ($\text{CaCl}_2 \cdot 2\text{H}_2\text{O}$, >99.5%) and copper chloride dihydrate ($\text{CuCl}_2 \cdot 2\text{H}_2\text{O}$, >99.5%) were purchased from Sigma-Aldrich and were of analytical grade. Tl(I) stock solution was prepared by dissolving TiNO_3 into deionized (DI) water and working solutions were freshly prepared by diluting Tl(I) stock solution with DI water.

2.2. Preparation of adsorbent

A mixture solution containing $\text{Fe}(\text{NO}_3)_3 \cdot 9\text{H}_2\text{O}$ and $\text{FeSO}_4 \cdot 7\text{H}_2\text{O}$ with the molar ratio of 2:1 was stirred under N_2 protection at $80 \text{ }^\circ\text{C}$, and then NaOH solution was slowly dropwise added. The formed Fe_3O_4 particles were collected, washed by DI water for several times and freeze-dried. After that, 50 mg of Fe_3O_4 powder was added into 30 mL ethanol and homogeneously dispersed by ultrasonication. Then, 30 mL titanium butoxide/ethanol solution was added under ultrasonication. The mixture solution was transferred into a 100-mL Teflon-line autoclave at $180 \text{ }^\circ\text{C}$ for 2 days. The produced crystal particles were washed and dried overnight at $60 \text{ }^\circ\text{C}$. In addition, TiO_2 was prepared through the same method except adding Fe_3O_4 powder.

2.3. Characterization of adsorbent

The surface morphology of the adsorbent was observed by SEM (ZEISS EVO18, Germany). The zeta potential and size distribution of the particles were determined by dynamic light scattering (Zetasize

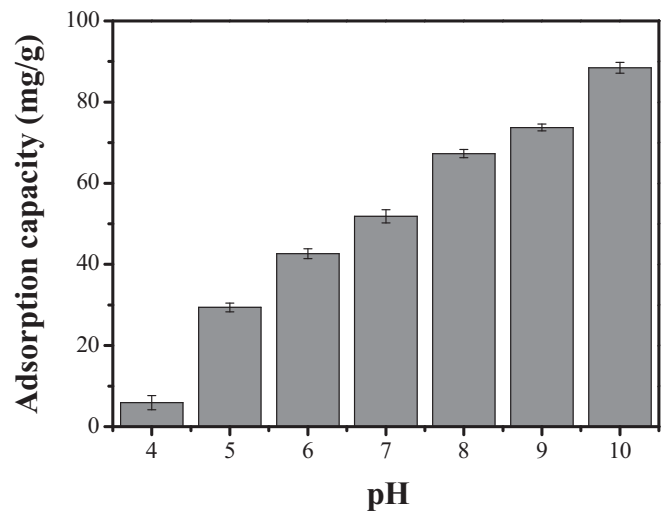


Fig. 4. Effect of solution pH on Tl(I) adsorption. Experiment conditions: $[Tl(I)]_0 = 12.5 \text{ mg/L}$; adsorbent dosage = 0.1 g/L; $T = 25 \pm 1 \text{ }^\circ\text{C}$.

nano ZSE, Malvern, UK). The solution pH at which the zeta potential equals zero is named as the isoelectric point (IEP), which is widely used to characterize the equilibrium of protonation and deprotonation of surface functional groups on the adsorbent. At the pH value of IEP, the adsorbent surface is considered to be neutrally charged. A BET surface analyzer (Aotosorb-iQ-MP/XR, USA) was used to measure specific surface areas of Fe_3O_4 particles and TFNPs by using the nitrogen adsorption isotherm technique. XRD measurements were performed on a Bruker D2 Phaser using the $K\alpha$ line of a Cu source with 2θ scan range of $20\text{--}80^\circ$ and a step size of 0.02° . Surface element distribution, element valence states and functional group composition of the adsorbents before and after the adsorption were determined by XPS (Kratos XPS system-Axis His-165 Ultra, Shimadzu, Japan). The magnetism of Fe_3O_4 particles and TFNPs was measured using a vibrating sample magnetometer (VSM, Lake Shore 7400, USA). The adsorbent after adsorption was collected using centrifuge, washed by DI for at least 3 times and dried in oven overnight for the XPS analysis. The XPS results were collected in the binding energy form and fitted with linear backgrounds and mixed functions composed of Gaussian (20%) and Lorentzian (80%) by using XPSPEAK 41 Software. To eliminate any charging effect, all spectra were corrected according to the binding energy of the C 1 s of graphite carbon at 284.8 eV.

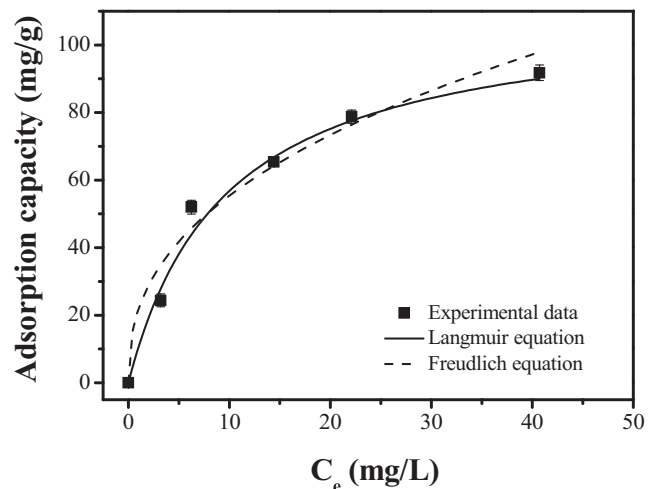


Fig. 5. Adsorption isotherm of Tl(I) on TFNPs. Experiment conditions: pH = 7.0; adsorbent dosage = 0.1 g/L; $T = 25 \pm 1 \text{ }^\circ\text{C}$.

Table 1
Constants of adsorption kinetics models.

Tl(I)	Pseudo-first-order			Pseudo-second-order		
	q_e (mg/g)	K_1 (h^{-1})	r^2	q_e (mg/g)	K_2 ($\text{g} \cdot \text{mg}^{-1} \cdot \text{h}^{-1}$)	r^2
24 h	52.1	3.779	0.92	52.1	0.136	0.98

Table 2
Langmuir and Freundlich isotherms parameters for Tl(I) adsorption.

	Langmuir isotherm			Freundlich isotherm		
	q_{max} (mg/g)	b (L/mg)	r^2	K_f (mg ^(1-1/n) L ^{1/n} /g)	$1/n$	r^2
Tl(I)	111.3	0.110	0.98	21.68	0.401	0.95

2.4. Adsorption experiments

Adsorption kinetics study was carried out at the initial Tl(I) concentration of 12.5 mg/L and solution pH was controlled at 7.0 throughout the experiment by adding HNO₃ or NaOH. The adsorbent dosage was 0.1 g/L. Samples were taken at predetermined times during the experiment. After filtered through 0.45 μm syringe filters, the concentration of thallium in samples was measured using an inductively coupled plasma mass spectrometry (ICP-MS).

The effect of solution pH on Tl(I) adsorption was conducted by adjusting 12.5 mg/L Tl(I) solutions to designated pH values in the range of 4.0–10.0. After adding the adsorbent with the dosage of 0.1 g/L, the suspension was stirred for 24 h at room temperature. Other procedures (e.g., sampling and concentration measurement) were the same as those in kinetics study. In order to further understand the role of Fe₃O₄ and TiO₂ on the removal of Tl(I), the adsorption capacities of Fe₃O₄ and TiO₂ under different solution pH were determined through the same procedure as mentioned above.

In the adsorption isotherm experiments, a series of working solutions were prepared with different initial Tl(I) concentrations varied from 5 to 150 mg/L. The adsorbent dosage was 0.1 g/L, and solution pH was maintained at 7.0 during the experiment. Other experimental steps were the same as those in kinetics study.

The influence of typical co-existing cations such as Na⁺, Mg²⁺, Ca²⁺ and Cu²⁺ on the Tl(I) adsorption was investigated by respectively adding a certain amount of NaCl, MgCl₂·6H₂O, CaCl₂·2H₂O and CuCl₂·2H₂O into 12.5 mg/L Tl(I) solutions. The solution pH was adjusted to 5.0, and the adsorbent dosage was 0.1 g/L. Other experimental operations were the same as aforementioned.

Three-cycle regeneration experiments were conducted to evaluate the reusability of the adsorbent. The spent adsorbent was collected by vacuum filtration and then regenerated using 0.1 M HNO₃ solution under stirring for 3 h. The regenerated adsorbent was washed by DI water and used for the next cycle of adsorption experiment. The adsorbent dosage was 0.1 g/L, and the solution pH was 7.0.

3. Results and discussion

3.1. Properties of adsorbent

From the SEM image as shown in Fig. 1a, the adsorbent with rough surface morphology is aggregated by numerous nano-sized particles

after heat-drying process. The isoelectric point (IEP) of TFNPs is determined as 4.8 according to Fig. 1b. As well known, the surface charge of the adsorbent is of high dependence on solution pH and can play a certain role in the adsorption process (Li et al., 2009). When solution pH is above IEP, the adsorbent becomes negatively charged due to the deprotonation of functional groups on the adsorbent surface. The strong electrostatic attraction between active sites and cationic thallium would facilitate the diffusion of Tl(I) towards the adsorbent and the adsorption reaction. On the contrary, the positively charged adsorbent surface formed at pH below IEP would be unfavorable for the adsorption of Tl(I) (Li et al., 2018b). A certain amount of Fe₃O₄, TiO₂ and TFNPs without drying treatment were homogeneously dispersed into DI water for the analysis of particle size distribution. As shown in Fig. 1c, the average volume diameter of Fe₃O₄, TiO₂ and TFNPs is 1023.4, 531.1 and 379.6 nm, respectively. It is worthwhile to note that TFNPs has smaller particle size than Fe₃O₄ and TiO₂, indicating that the Fe₃O₄ magnetic particles can be effectively transformed into smaller ones during the hydrothermal reaction. This might be due to the fact that aggregated Fe₃O₄ magnetic particles after heat-drying process could be further broken up under the high temperature and pressure of hydrothermal reaction. The BET specific surface areas of Fe₃O₄ particles and TFNPs are 85.5 and 289.3 m²/g, respectively. The XRD patterns of Fe₃O₄, TiO₂ and TFNPs are illustrated in Fig. 1d. The characteristic peaks at 30.1°, 35.5°, 43.1°, 57.0° and 62.6° can be assigned to the XRD diffraction of pure Fe₃O₄ crystal (Yang et al., 2010; PDF No. 88-0315). In the XRD pattern of TiO₂, the presence of two broad peaks at about 25.3° and 50.6° indicates that the TiO₂ particle is poorly crystallized. All the characteristic peaks of Fe₃O₄ crystal can be observed in the XRD pattern of TFNPs but the corresponding peaks become broaden and weaken, suggesting that no significant phase change occurs and the incorporation of titanium oxide may obscure the XRD signals of Fe₃O₄ particles.

As shown in Fig. 2, the saturation magnetism of Fe₃O₄ is measured as 64.5 emu/g, while the value of TFNPs is decreased to around 30.8 emu/g due to the surface modification of TiO₂. The sufficient magnetism of TFNPs should be beneficial for their magnetic separation after the adsorption process.

3.2. Adsorption kinetics

The adsorption rate is of crucial importance for the practical application of an adsorbent. As shown in Fig. 3, approximately 83% of ultimate adsorption capacity (43.0 mg/g) of Tl(I) can be achieved in the first 30 min and the adsorption equilibrium is reached within 6 h at the initial Tl(I) concentration of 12.5 mg/L.

The adsorption data was further simulated by the pseudo-first-order and pseudo-second-order models. The mathematical equations are expressed as below:

$$\ln(q_e - q_t) = \ln q_e - K_1 t \quad (1)$$

$$t/q_t = 1/(K_2 q_e^2) + t/q_e \quad (2)$$

Table 3
Adsorption capacities of Tl(I) on previously reported adsorbents.

Adsorbent	Tl(I) conc. rang (mg/L)	pH	Dosage (g/L)	Max. adsorption capacity (mg/g)	Reference
Treated sawdust	0–1000	7.0	100	13.18	(Memon et al., 2008)
Multiwalled carbon nanotube	0–0.12	6.0	0.1	0.42	(Pu et al., 2013)
Polyacrylamide-zeolite	2–2000	5.0	10	378.1	(Şenol and Ulusoy, 2010)
Polyacrylamide-bentonite	2–2000	5.0	10	73.6	(Şenol and Ulusoy, 2010)
Titanium peroxide	5–130	7.0	0.2	412	(Zhang et al., 2018)
Titanium dioxide	5–130	7.0	0.2	258	(Zhang et al., 2018)
Titanate nanotube	0–60	5.0	0.2	709.2	(Liu et al., 2014)
Prussian blue-alginate capsules	0–400	4.0	1.0	103.0	(Vincent et al., 2014)
MnO ₂ @pyrite cinder	0–160	12.0	0.5	320.1	(Li et al., 2018b)
TFNPs	0–150	7.0	0.1	111.3	This study

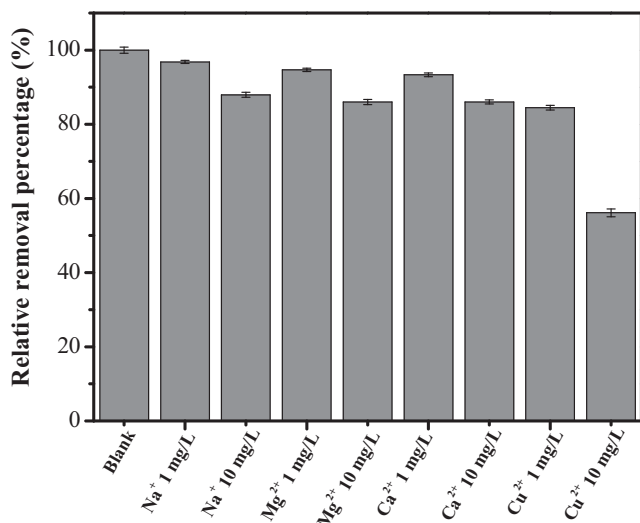


Fig. 6. Effect of co-existing cations on Tl(I) uptake. Experiment conditions: $[Tl(I)]_0 = 12.5$ mg/L; adsorbent dosage = 0.1 g/L; $T = 25 \pm 1$ °C; $pH = 5.0$.

where q_e and q_t are the adsorption amount of Tl(I) on the adsorbent at equilibrium and time t (mg/g), K_1 (h^{-1}) and K_2 ($g \cdot mg^{-1} \cdot h^{-1}$) are the parameters of the pseudo-first-order and pseudo-second-order models, respectively, and t is the time (h).

As illustrated in Table 1, the pseudo-second-order kinetics model works better to fit the experimental data than the pseudo-first-order kinetics model according to the values of r^2 . This suggests that chemical adsorption process might be involved in the uptake of Tl(I) on the adsorbent.

The adsorption process generally includes the external diffusion (diffusion from bulk solution through solid-liquid interfacial film to the adsorbent's exterior surface), intraparticle diffusion (diffusion into the adsorbent's interior pores) and adsorption on the active sites (Srivastava et al., 2013). Since the chemisorption step is very rapid, the adsorption rate of Tl(I) on the adsorbent might be limited by the external diffusion and/or intraparticle diffusion. Therefore, the intraparticle diffusion model was employed for simulating the experimental data to find out the rate-limiting step. The equation is expressed as below:

$$q_t = K_{id}t^{1/2} + \alpha \quad (3)$$

where q_t (mg/g) is the adsorption amount of Tl(I) on the adsorbent at time t , K_{id} ($mg \cdot g^{-1} \cdot h^{-1/2}$) is the intraparticle diffusion rate constant, α (mg/g) refers to the boundary layer effect, and t is the time (h).

As shown in Fig. S1, the plot of q_t vs $t^{1/2}$ gives a multilinearity that indicates the adsorption of Tl(I) involves a multi-step process. The first linear stage within 2 h represents the intraparticle diffusion step and the second one reveals the adsorption equilibrium step (Ning et al., 2012). It is noted that the value of α in the first linear stage is as high as 26.5 mg/g, approximately 50% of the equilibrium adsorption capacity as seen from Table S1. A higher α value

Table 4
Ionic properties of cations used in this study^a.

Metal ion	Electronegativity	Ionic radius (Å)	Hydrated ionic radius (Å)
Na(I)	0.93	1.02	3.58
Mg(II)	1.31	0.72	4.28
Ca(II)	1.00	0.99	4.12
Cu(II)	1.90	0.73	4.19
Tl(I)	1.62	1.50	3.30

^a Electronegativity, ionic radius and hydrated ionic radius cited from the literature (Kinraide and Yermiyahu, 2007).

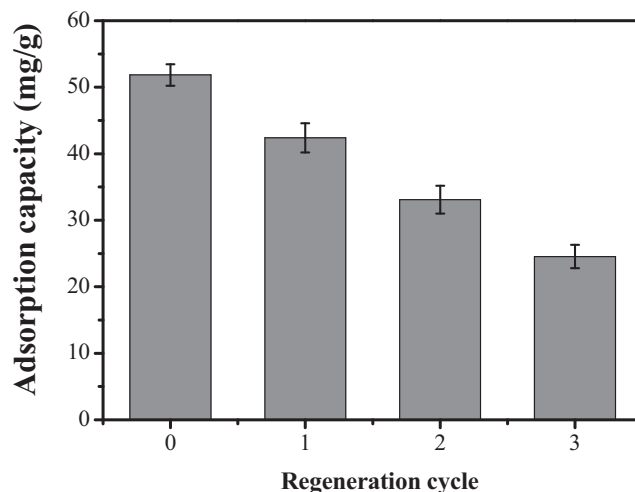


Fig. 7. Regeneration study of the adsorbent. Experiment conditions: $[Tl(I)]_0 = 12.5$ mg/L; adsorbent dosage = 0.1 g/L; $T = 25 \pm 1$ °C; $pH = 7.0$.

from the equation reflects that the boundary layer effect has a more significant effect on the adsorption kinetics. Therefore, it can be concluded that the adsorption rate of Tl(I) on the adsorbent is mainly limited by the external diffusion and intraparticle diffusion. Only about 10% of ultimate adsorption capacity is achieved at the adsorption equilibrium step. The slow-down adsorption rate in this stage is caused by the great reduction of the Tl(I) concentration in liquid phase.

3.3. pH effect

The effect of solution pH on the uptake of Tl(I) was studied and the results are given in Fig. 4. It can be seen that the adsorption capacity of Tl(I) is gradually increased with the increase of solution pH. The optimal adsorption of Tl(I) is accomplished at pH 10.0. Similar phenomenon was observed in the adsorption of Tl(I) on other titanium-based adsorbents (e.g., titanate nanotube (Liu et al., 2014) and titanium peroxide (Zhang et al., 2018)). As shown in Fig. S2, existing form of Tl(I) in water is monovalent cation (Tl^+) in the tested pH range of 4.0–10.0. Based on the results of zeta potential measurement, the surface charge of the adsorbent will

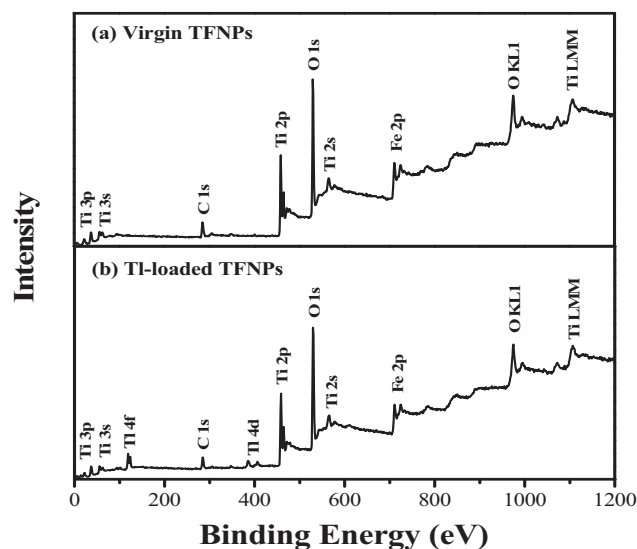


Fig. 8. XPS wide-scan spectra of the adsorbents before and after Tl(I) adsorption.

become positive at $\text{pH} < 4.8$, leading to the occurrence of electrostatic repulsion between the positively charged adsorbent and Ti^+ ions (Li et al., 2018b). The adsorption capacity of $\text{Ti}(\text{I})$ on the adsorbent is therefore retarded at $\text{pH} 4.0$. When solution pH is above 4.8, the adsorbent surface turns to be negatively charged and negative charge density on the adsorbent surface increases with increasing solution pH due to the successive deprotonation of functional groups. The enhanced electrostatic attraction between the adsorbent and $\text{Ti}(\text{I})$ at such pH conditions should be beneficial for the adsorption of $\text{Ti}(\text{I})$ (Pu et al., 2013; Liu et al., 2014).

The adsorption capacities of Fe_3O_4 and TiO_2 at solution pH ranging from 4.0 to 10.0 are shown in Fig. S3. The tendency of the adsorption of $\text{Ti}(\text{I})$ on Fe_3O_4 and TiO_2 is similar to that on TFNPs, and the TiO_2 performs much better than Fe_3O_4 on the $\text{Ti}(\text{I})$ removal in the whole pH range. The adsorption capacities of Fe_3O_4 and TiO_2 at $\text{pH} 7.0$ are 13.1 and 65.2 mg/g , respectively. This indicates that both Fe_3O_4 and TiO_2 in TFNPs might be involved in the adsorption process of $\text{Ti}(\text{I})$.

3.4. Adsorption isotherm

The adsorption isotherm of $\text{Ti}(\text{I})$ on the adsorbent at $\text{pH} 7.0$ with the fitting by the Langmuir and the Freundlich equations is shown in Fig. 5. One can see that the adsorbent can effectively remove $\text{Ti}(\text{I})$ from water. According to the parameters listed in Table 2, the Langmuir equation is more suitable for describing the experimental data than the Freundlich equation. This suggests that the adsorption of $\text{Ti}(\text{I})$ on the adsorbent is mainly governed by a monolayer adsorption process (Zhao et al., 2016; Yu et al., 2019). The maximum adsorption capacity calculated by the Langmuir equation is 111.3 mg/g at $\text{pH} 7.0$. A comparison between TFNPs and previously reported adsorbents for the $\text{Ti}(\text{I})$ removal is illustrated in Table 3. It is demonstrated that TFNPs can work as an efficient adsorptive material for thallium decontamination with the advantages of rapid adsorption rate and facile magnetic separation capability.

3.5. Effect of co-existing cations

Since a variety of cations such as Na^+ , Mg^{2+} , Ca^{2+} and Cu^{2+} may co-exist in water and compete for the active sites on the adsorbent with $\text{Ti}(\text{I})$, it is important to evaluate the effect of these cations on the adsorption of $\text{Ti}(\text{I})$. As shown in Fig. 6, the negative effect of the presence of co-existing cations becomes more obvious with increasing their concentrations. However, the presence of Na^+ , Mg^{2+} and Ca^{2+} is found to have slight influence in the uptake of $\text{Ti}(\text{I})$. Compared to the blank sample, the adsorption capacity of $\text{Ti}(\text{I})$ is respectively reduced by approximately 12.0%, 13.9% and 14.0% when the concentrations of Na^+ , Mg^{2+} and Ca^{2+} are as high as 10 mg/L . Similar to the study reported by Zhang et al. (2018), the presence of Cu^{2+} seems to cause a more significant depression effect on the uptake of $\text{Ti}(\text{I})$. Approximately 43.8% of reduction in the adsorption capacity of $\text{Ti}(\text{I})$ is observed at the copper concentration of 10 mg/L . The specific affinity of metal ions towards functional groups on the adsorbent (e.g., $-\text{OH}$) is reportedly dependent on ionic properties including ionic potential, ionic radius, electronegativity and softness parameters (Depci et al., 2012; Zhang et al., 2018). The relevant ionic properties of cations used in this study are illustrated in Table 4. The influence of co-existing cations on the uptake of $\text{Ti}(\text{I})$ seems to be greatly affected by the electronegativity. The electronegativity of $\text{Cu}(\text{II})$ is higher than other metal cations, leading to stronger competition with $\text{Ti}(\text{I})$ for the active sites.

3.6. Reusability of adsorbent

As shown in Fig. 7, the reusability of the adsorbent was evaluated by three-cycle adsorption and regeneration experiments at $\text{pH} 7.0$. The

adsorption capacity of the adsorbent in Cycle 0 represents that of the virgin adsorbent. Approximately 81.8% of initial adsorption capacity can be recovered after the first regeneration cycle. The adsorption capacity is still maintained at about 47.4% of the virgin adsorbent after three regeneration cycles.

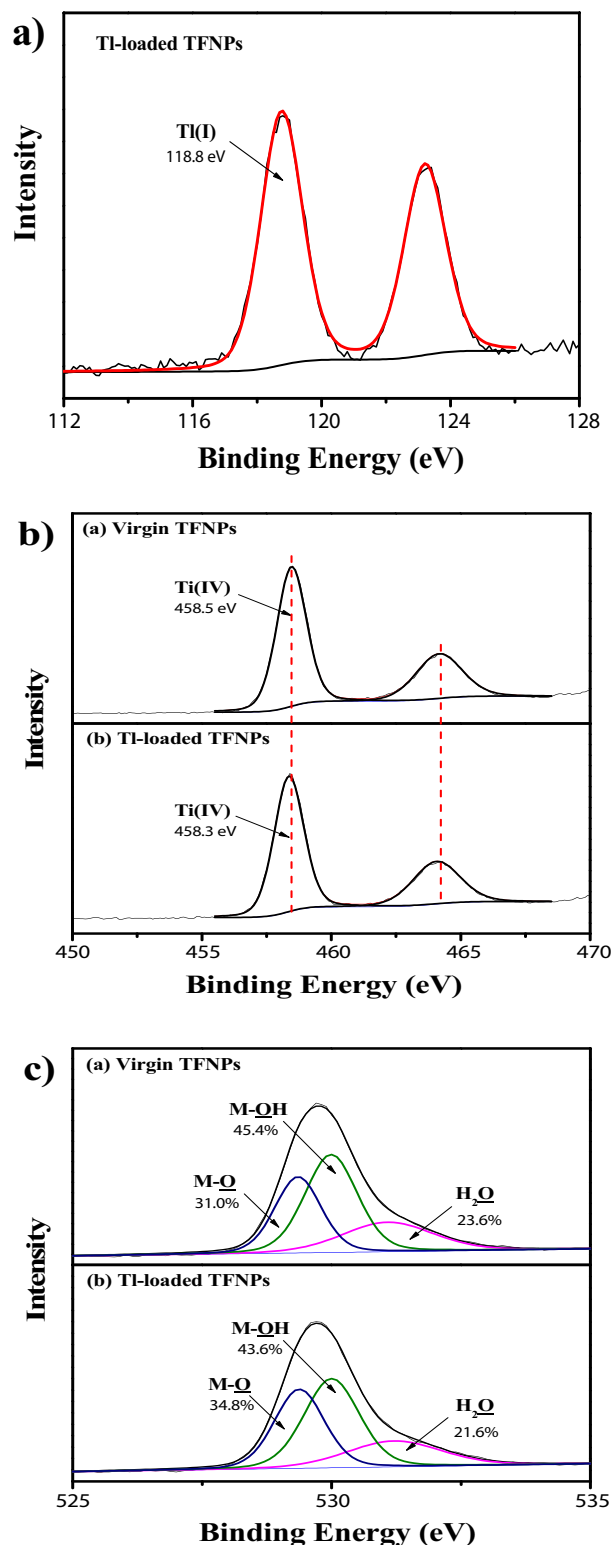


Fig. 9. High-resolution XPS spectra of the adsorbents before and after adsorption: (a) $\text{Ti} 4f$, (b) $\text{Ti} 2p$ and (c) $\text{O} 1s$.

3.7. Adsorption mechanism

As shown in Fig. 8, the characteristic peaks of titanium and iron including Ti 3p, Ti 3 s, Ti 2p, Ti 2 s, Ti LMM and Fe 2p can be detected in the wide-scan XPS spectrum of virgin TFNPs. After the adsorption, two new peaks assigned to Ti 4f and Ti 4d appear on the XPS spectrum of Ti(I)-loaded TFNPs, indicating that Ti(I) has been effectively adsorbed on the adsorbent surface.

The thallium element valence after the adsorption was determined by XPS analysis. As seen from Fig. 9a, the characteristic peak of Ti 4f with the binding energy of 118.8 eV can be attributed to Ti(I) (Wan et al., 2014), suggesting that there is no redox reaction of Ti(I) occurred on the adsorbent surface.

The high-resolution Ti 2p XPS spectra of the adsorbents before and after adsorption of Ti(I) are given in Fig. 9b. The oxidation state of titanium element on the virgin adsorbent is identified as +IV according to its binding energy of 458.5 eV. After the adsorption, the binding energy shifts to a lower position (458.3 eV) probably due to the attachment of positively charged Ti(I) ions. This indicates that the oxidation state of titanium is not changed during the adsorption and Ti(I) ions are chemically adsorbed on the active sites that are linked to titanium atoms. As shown in Fig. S4, the Fe 2p core-level XPS spectrum of virgin adsorbent can be decomposed into five component peaks with the binding energies of 709.7, 717.2, 711.5, 713.9 and 719.7 eV, respectively assigned to Fe(II)_{oct}, Fe(II)_{sat}, Fe(III)_{oct}, Fe(III)_{tet}, and Fe(III)_{sat} (Wan et al., 2014). According to the relative contents listed in Table S2, the molar ratio of Fe(II)/Fe(III) is close to 0.5 as expected value of Fe₃O₄ particles. Similar to titanium element, binding energies of aforementioned peaks also slightly shift to lower levels, indicating the bonding of Ti(I) ions to iron atoms.

The O 1s core-level XPS spectra of the virgin and Ti(I)-loaded adsorbents in Fig. 9c can be divided into three peaks of metal oxygen bond (M-O), metal-hydroxyl group (M-OH) and the adsorbed water (H₂O). After the Ti(I) adsorption, the relative content of M-O bond increases from 31.0% to 34.8%, while the contents of M-OH bond and H₂O decrease from 45.4% to 43.6% and 23.6% to 21.6%, respectively.

Based on experimental data and results from XPS analysis, a possible mechanism for Ti(I) adsorption could be deduced. The hydroxyl groups bonded to Ti or Fe atoms should be highly involved in the uptake of Ti(I). The protonation or deprotonation of hydroxyl groups could significantly affect the diffusion of Ti(I) towards the active sites. At pH above 4.8, the electrostatic attraction between the adsorbent and Ti(I) ions would play a certain role in the Ti(I) uptake, and Ti(I) ions are adsorbed on the adsorbent surface through the formation of inner-surface complexes.

4. Conclusions

The titanium iron magnetic adsorbent was aggregated by nano-sized particles after heat-drying procedure. The adsorbent exhibited more favorable uptake of Ti(I) with increasing the solution pH. Both kinetics and isotherm studies demonstrated that the adsorption of Ti(I) was govern by a chemisorption process and the maximum adsorption capacity at pH 7.0 could reach 111.3 mg/g, much higher than most of adsorbents previously reported. The influence of other co-existing cations on the Ti(I) adsorption was mainly determined by their electronegativity. The presence of Cu²⁺ showed the most significant interference on the uptake of Ti(I). Mechanism study indicated that the hydroxyl groups on the adsorbent surface played a key role in the adsorption process. During the adsorption, the Ti(I) ions could effectively and rapidly bonded with deprotonated hydroxyl groups and adsorbed on the adsorbent surface through the mechanism of surface complexation. Due to its excellent adsorption performance and ease in operation, the synthesized magnetic adsorbent could be considered as a better material for the thallium decontamination.

Acknowledgments

This research was supported by Natural Science Foundation of Guangdong Province (Grant No. 2018A0303130148) and Guangzhou Science and Technology Program (Grant No. 201704020138).

Appendix A. Supplementary data

Supplementary data to this article can be found online at <https://doi.org/10.1016/j.scitotenv.2019.133625>.

References

- Campanella, B., Casiot, C., Onor, M., Perotti, M., Petrini, R., Bramanti, E., 2017. Thallium release from acid mine drainages: speciation in river and tap water from Valdicastello mining district (northwest Tuscany). *Talanta* 171, 255–261.
- Chandra, V., Park, J., Chun, Y., Lee, J.W., Hwang, I.C., Kim, K.S., 2010. Water-dispersible magnetite-reduced graphene oxide composites for arsenic removal. *ACS Nano* 4, 3979–3986.
- Cheam, V., Lechner, J., Desrosiers, R., Sekerka, I., Lawson, G., Mudroch, A., 1995. Dissolved and total thallium in Great Lakes waters. *J. Great Lakes Res.* 21, 384–394.
- Depci, T., Kul, A.R., Önal, Y., 2012. Competitive adsorption of lead and zinc from aqueous solution on activated carbon prepared from Van apple pulp: study in single- and multi-solute systems. *Chem. Eng. J.* 200–202, 224–236.
- Feng, Y., Gong, J.L., Zeng, G.M., Niu, Q.Y., Zhang, H.Y., Niu, C.G., et al., 2010. Adsorption of Cd(II) and Zn(II) from aqueous solutions using magnetic hydroxyapatite nanoparticles as adsorbents. *Chem. Eng. J.* 162, 487–494.
- Kinraide, T.B., Yermiyahu, U., 2007. A scale of metal ion binding strengths correlating with ionic charge, Pauling electronegativity, toxicity, and other physiological effects. *J. Inorg. Biochem.* 101, 1201–1213.
- Li, H., Li, X., Chen, Y., Long, J., Zhang, G., Xiao, T., Zhang, P., Li, C., Zhuang, L., Huang, W., 2018a. Removal and recovery of thallium from aqueous solutions via a magnetite-mediated reversible adsorption-desorption process. *J. Clean. Prod.* 199, 705–715.
- Li, H., Li, X., Xiao, T., Chen, Y., Long, J., Zhang, G., Zhang, P., Li, C., Zhuang, L., Li, K., 2018b. Efficient removal of thallium(I) from wastewater using flower-like manganese dioxide coated magnetic pyrite cinder. *Chem. Eng. J.* 353, 867–877.
- Li, H., Li, X., Long, J., Li, K., Chen, Y., Jiang, J., Chen, X., Zhang, P., 2019. Oxidation and removal of thallium and organics from wastewater using a zero-valent-iron-based Fenton-like technique. *J. Clean. Prod.* 221, 89–97.
- Li, Y., Gao, B., Wu, T., Sun, D., Li, X., Wang, B., Lu, F., 2009. Hexavalent chromium removal from aqueous solution by adsorption on aluminum magnesium mixed hydroxide. *Water Res.* 43, 3067–3075.
- Lin, T.S., Nriagu, J., 1999. Thallium speciation in the Great Lakes. *Ann. Hum. Genet.* 50, 259–270.
- Liu, W., Zhang, P., Borthwick, A.G.L., Chen, H., Ni, J., 2014. Adsorption mechanisms of thallium(I) and thallium(III) by titanate nanotubes: ion-exchange and co-precipitation. *J. Colloid Interface Sci.* 423, 67–75.
- Memon, S.Q., Memon, N., Solangi, A.R., Memon, J.U.R., 2008. Sawdust: a green and economical sorbent for thallium removal. *Chem. Eng. J.* 140, 235–240.
- Mulkey, J.P., Oehme, F.W., 1993. A review of thallium toxicity. *Vet. Hum. Toxicol.* 35, 445–453.
- Ning, L., Zheng, M., Wei, X., 2012. Study on sorption of chlorophenols from aqueous solutions by an insoluble copolymer containing β -cyclodextrin and polyamidoamine units. *Chem. Eng. J.* 192, 138–145.
- Ning, W., Xu, Z., Xu, W., Jing, X., Chen, Y., Min, Z., 2018. Comparison of coagulation and magnetic chitosan nanoparticle adsorption on the removals of organic compound and coexisting humic acid: a case study with salicylic acid. *Chem. Eng. J.* 347, 514–524.
- Pan, S., Shen, H., Xu, Q., Luo, J., Hu, M., 2012. Surface mercapto engineered magnetic Fe₃O₄ nanoadsorbent for the removal of mercury from aqueous solutions. *J. Colloid Interface Sci.* 365, 204–212.
- Peter, A.L.J., Viraraghavan, T., 2005. Thallium: a review of public health and environmental concerns. *Environ. Int.* 31, 493–501.
- Pu, Y., Yang, X., Hong, Z., Wang, D., Yu, S., Jie, H., 2013. Adsorption and desorption of thallium(I) on multiwalled carbon nanotubes. *Chem. Eng. J.* 219, 403–410.
- Ralph, L., Twiss, M.R., 2002. Comparative toxicity of thallium(I), thallium(III), and cadmium(II) to the unicellular alga *Chlorella* isolated from Lake Erie. *Bull. Environ. Contam. Toxicol.* 68, 261–268.
- Rivera-Utrilla, J., Ferro-García, M.A., Mata-Arjona, A., González-Gómez, C., 2010. Studies on the adsorption of caesium, thallium, strontium and cobalt radionuclides on activated carbons from aqueous solutions. *J. Chem. Technol. Biotechnol.* 34, 243–250.
- Şenol, Z.M., Ulusoy, U., 2010. Thallium adsorption onto polyacryamide–aluminosilicate composites: a TI isotope tracer study. *Chem. Eng. J.* 162, 97–105.
- Srivastava, P., Goyal, S., Tayade, R., 2013. Ultrasound-assisted adsorption of reactive blue 21 dye on TiO₂ in the presence of some rare earths (La, Ce, Pr & Gd). *Can. J. Chem. Eng.* 92, 41–51.
- Tang, W., Yu, S., Qi, L., Gao, S., Jian, K.S., 2013. Superparamagnetic magnesium ferrite nanoadsorbent for effective arsenic (III, V) removal and easy magnetic separation. *Water Res.* 47, 3624–3634.
- Vincent, T., Taulemesse, J.M., Dauvergne, A., Chanut, T., Testa, F., Guibal, E., 2014. Thallium (I) sorption using Prussian blue immobilized in alginate capsules. *Carbohydr. Polym.* 99, 517–526.

- Wan, S., Ma, M., Lv, L., Qian, L., Xu, S., Xue, Y., et al., 2014. Selective capture of thallium (I) ion from aqueous solutions by amorphous hydrous manganese dioxide. *Chem. Eng. J.* 239, 200–206.
- Williams-Beam, C., Twidwell, L.G., 2003. Removal of thallium from wastewater. *Electro-metallurgy and Environmental Hydrometallurgy*.
- Yang, Z.P., Gong, X.Y., Zhang, C.J., 2010. Recyclable Fe_3O_4 /hydroxyapatite composite nanoparticles for photocatalytic applications. *Chem. Eng. J.* 165, 117–121.
- Yu, L., Yu, Y., Li, J., Chen, J.P., 2019. Development and characterization of yttrium-ferrocyanide binary composite for treatment of highly concentrated arsenate wastewater. *J. Hazard. Mater.* 361, 348–356.
- Zhang, G., Fang, F., Li, X., Qi, J., Chen, Y., 2018. Superior adsorption of thallium(I) on titanium peroxide: performance and mechanism. *Chem. Eng. J.* 331, 471–479.
- Zhang, L., Huang, T., Zhang, M., Guo, X., Yuan, Z., 2008. Studies on the capability and behavior of adsorption of thallium on nano- Al_2O_3 . *J. Hazard. Mater.* 157, 352–357.
- Zhang, S., Li, X.Y., Chen, J.P., 2010. Preparation and evaluation of a magnetite-doped activated carbon fiber for enhanced arsenic removal. *Carbon* 48, 60–67.
- Zhao, D., Yu, Y., Chen, J.P., 2016. Treatment of lead contaminated water by a PVDF membrane that is modified by zirconium, phosphate and PVA. *Water Res.* 101, 564–573.